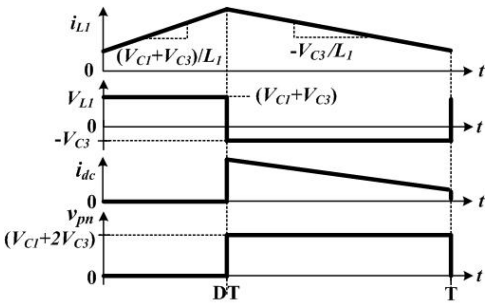


Fig. 4. Waveforms of the proposed MCA-ZSI.

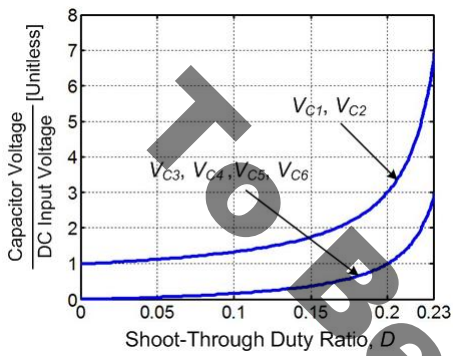


Fig. 5. Capacitor voltage stress ratio of the proposed MCA-ZSI with various shoot-through duty ratios.

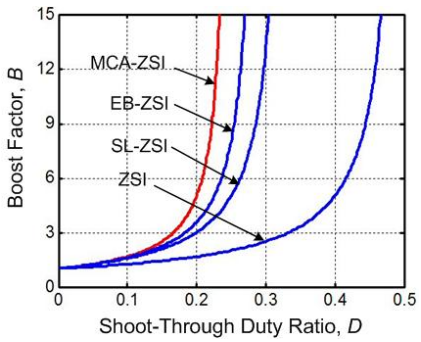


Fig. 6. Boost factors of four topologies.

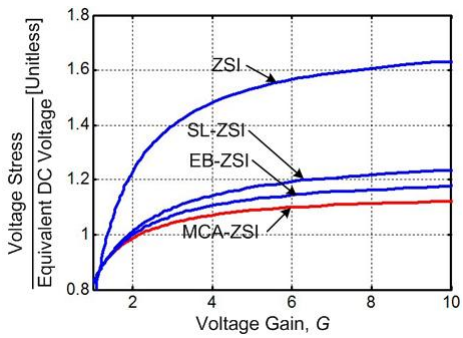


Fig. 7. Voltage stress ratio of four topologies.

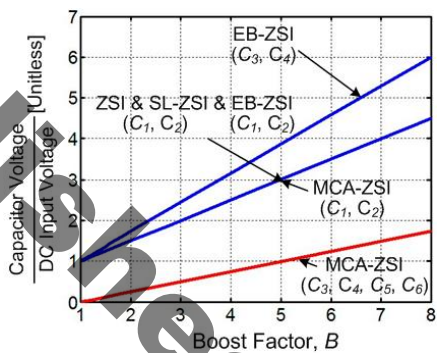


Fig.8. Capacitor voltage stress ratio of four topologies.

as the dc input power is identical to the dc-link power such as $V_{dc} \cdot i_{dc} = \hat{v}_{pn} \cdot I_i$, the dc-link current in the non-shoot-through state is expressed as the dc input current.

$$I_i = \frac{1-5D+4D^2}{1-D} i_{dc} . \quad (18)$$

Substituting (18) into (17), the current stress of four inductors can be expressed as the shoot-through duty ratio and dc input current.

$$\bar{i}_L = (1-D) i_{dc} \quad (19)$$

### *B. Modulation Technique*

A modulation scheme for the proposed topology focuses on efficiently embedding the shoot-through state within a zero state for enhancing a boost ability while the active state remains fixed. The ac output gain is dependent on a mixture between *M* and *B* from (16). Because one switching period is shared by the non-shoot-through state and the shoot-through state, the ac output gain has influence on the modulation techniques owing to the trade-off between *M* and *D*. Among three carrier-based modulation techniques such as simple control, constant boost control, and maximum boost control techniques [20], the constant boost control technique reported in [21] is utilized at the proposed topology for removing the low-frequency voltage and current ripples and getting a higher voltage boosting ability with the lower possible value of *D*.

Because the maximum modulation index with a given *D* can be drawn out as $M = (2/\sqrt{3})(1-D)$ by using the constant boost control method, a higher ac output voltage with a given low *D* can be produced.

## IV. Comparison of the Proposed MCA-ZSI with Other Topologies

This section describes a comparison analysis of performances among the proposed MCA-ZSI, traditional ZSI, SL-ZSI, and EB-ZSI. These topologies are compared to their

boost factor, voltage stress of inverter switching devices, capacitor voltage stress, and the number of components utilized at the impedance network.

Fig. 6 shows the boost factors of four topologies according to a variation of shoot-through duty ratio. Among four topologies, the proposed MCA-ZSI has the highest boost factor in the total range of the shoot-through duty ratio. Therefore, the proposed MCA-ZSI can produce a higher ac output voltage with a lower shoot-through duty ratio. Fig. 7 shows the ratio of the voltage stress across inverter switches to the minimum dc input voltage with a variation of ac voltage gain $G$ for four topologies. It can be noted that the proposed MCA-ZSI has the lowest voltage stress across inverter switching devices among four topologies. It can save the cost of power converter. Fig. 8 shows the ratio of the capacitor voltage stress to the dc input voltage with various boost factors $B$ for four topologies. The voltage stress of two capacitors of the MCA-ZSI ($C_1$ and $C_2$) is the same as the voltage stress of two capacitors of the EB-ZSI, SL-ZSI, and traditional ZSI. The voltage stress of four capacitors of the MCA-ZSI ($C_3$, $C_4$, $C_5$, and $C_6$) is much lower than the capacitor voltage stress of the other topologies, and the two capacitors of the EB-ZSI ($C_3$ and $C_4$) have the highest capacitor voltage stress.

Table I reports the comparison of the number of passive components and diodes used at the impedance network in the proposed MCA-ZSI, EB-ZSI, SL-ZSI, and traditional ZSI. The number of inductors required at the MCA-ZSI, EB-ZSI, and SL-ZSI is identical. Although the proposed MCA-ZSI needs two or four capacitors more than the other three topologies, four of six capacitors have very low capacitor voltage stress. Additionally, two or four diodes can be saved. In conclusion, the total number of components utilized at the impedance network of the MCA-ZSI is the same as that of the other two topologies except the traditional ZSI, while the voltage stress of four capacitors of the MCA-ZSI is about 2.5 times lower than that of the other topologies.

TABLE I

NUMBER OF COMPONENTS AT IMPEDANCE NETWORK

| Topologies | Inductors | Capacitors | Diodes |
|---|---|---|---|
| MCA-ZSI | 4 | 6 | 3 |
| EB-ZSI | 4 | 4 | 5 |
| SL-ZSI | 4 | 2 | 7 |
| ZSI | 2 | 2 | 3 |

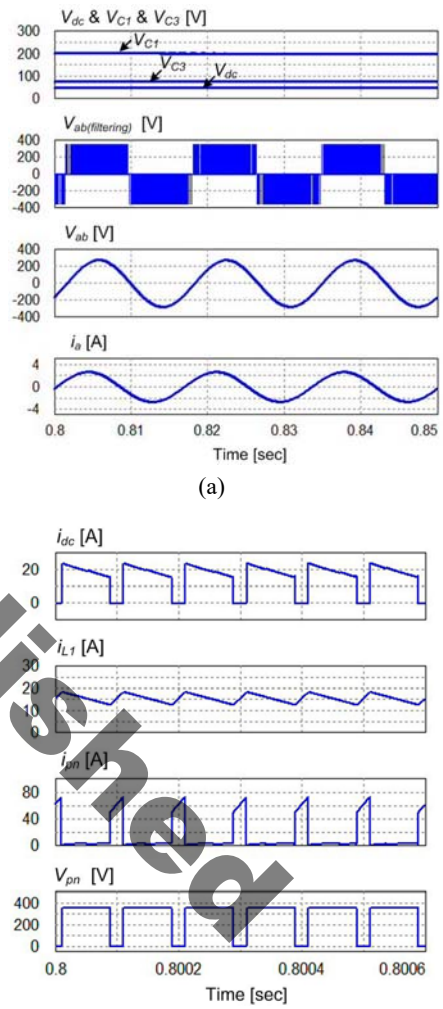


Fig. 9. Simulation waveforms of MCA-ZSI at $M$ = 0.91, $D$ = 0.214: (a) capacitor and dc input voltages, ac output voltage and current (b) dc input and inductor currents, dc-link current and voltage.

## V. SIMULATION AND EXPERIMENTAL RESULTS

In order to demonstrate the enhanced boost ability of the proposed topology, both the simulation and experiments are performed with the following circuit parameters:

- Impedance network: $L_1 = L_2 = L_3 = L_4 = 1$ mH; $C_1 = C_2 = C_3 = C_4 = C_5 = C_6 = 1000$ μF;
- Three-phase LC output filter: $L_f = 0.6$ mH, $C_f = 100$ μF;
- Three-phase resistive-inductance load: $R = 60$ Ω, $L = 1.2$ mH;
- Switching frequency = 5 kHz.

### A. Simulation results

The simulation studies are carried out on the open loop control of the proposed topology in PSIM program, neglecting the equivalent series resistances (ESRs) in the inductors and capacitors and the forward voltage drop of switching devices and diodes. Fig. 9 shows the simulation results when $M$ = 0.91, $D$ = 0.214, and $V_{dc}$ = 50 V. The capacitor voltages $V_{C1}$ and $V_{C3}$ are put up to 200 V and 75 V from the dc input voltage of 50 V, respectively, and the peak of dc-link voltage is 350 V. The ac output voltage with 190

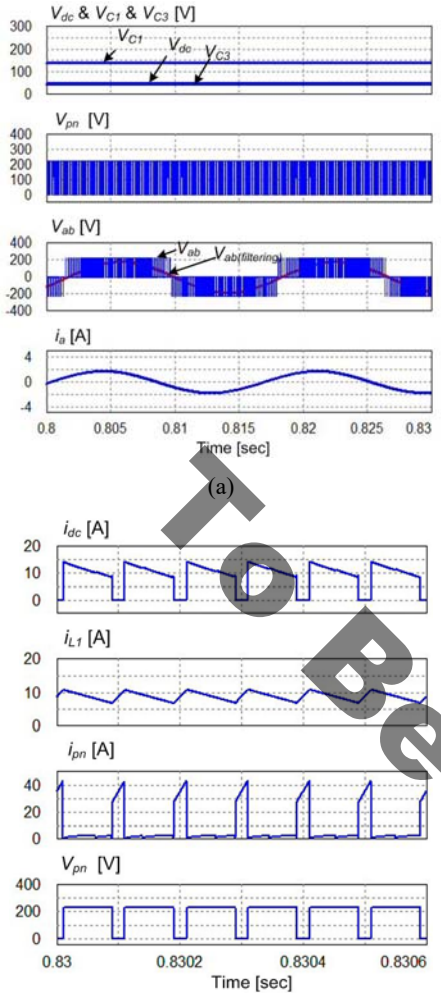


Fig. 10. Simulation waveforms of MCA-ZSI at $M$ = 0.93, $D$ = 0.195: (a) capacitor and dc input voltages, ac output voltage and current (b) dc input and inductor currents, dc-link current and voltage.

TABLE II
SUMMARY OF SIMULATION RESULTS

| Operating Conditions | $V_{C1}$ | $V_{C3}$ | $\hat{v}_{pn}$ | $V_{ab}$ | $\bar{i}_L$ |
|---|---|---|---|---|---|
| $M$ = 0.91<br>$D$ = 0.214 | 200 V | 75 V | 350 V | 190 V | 15 A |
| $M$ = 0.93<br>$D$ = 0.195 | 135 V | 45 V | 225 V | 225 V | 9 A |

Vrms can be produced. From Fig. 9(b), during shoot-through state, the dc input current is zero, and the inductor current increases while the dc-link voltage is zero. The dc-link voltage has a peak voltage and the inductor current decreases in non-shoot-through state. The average of inductor current is about 15 A, which can be calculated by multiplying the

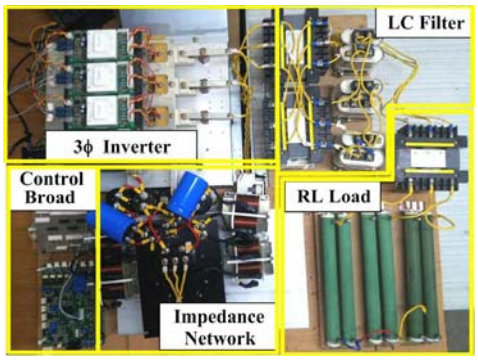


Fig. 11. Photograph of experimental system setup.

average of dc input current at non-shoot-through period, 19 A by the non-shoot-through duty ratio, (1 – $D$) = 0.786 from (19).

Fig. 10 shows the simulation waveforms when $M$ = 0.93, $D$ = 0.195 at the same dc input voltage as 50 V. As the shoot-through duty ratio is lowered from 0.214 to 0.195, the capacitor voltages $V_{C1}$ and $V_{C3}$ decrease from 200 V and 75 V to 135 V and 45 V, respectively, where $V_{C3}$ is slightly lower than the dc input voltage. The ac output voltage is shrunk to 128 Vrms in spite of increasing the modulation index $M$ from 0.91 to 0.93, because the dc-link voltage reduces from 350 V to 225 V as $D$ decreases from 0.21 to 0.195.

Table II describes the values of capacitor voltages, dc-link voltage, ac output voltages, and inductor current at the two operating conditions for summarizing simulation results.

### *B. Experimental Results*

In Fig. 11, the experimental system setup built in the laboratory is shown. It consists of three-phase inverter, impedance network, LC filter, RL load, and DSP control board. The 32-bit DSP TMS 320F28335 is utilized to generate the PWM signals including the shoot-through state.

Fig. 12 shows the experiment results at the identical operating conditions with the simulation results shown in Fig. 9. As shown in Fig. 12, the capacitor voltages $V_{C1}$, $V_{C3}$ are raised to 195 V and 72 V, respectively. The dc-link voltage can be put up to 6.8 times from 50 V dc input voltage, and the rms value of line-to-line voltage filtered by an LC filter is 185 V. The a-phase output current $i_a$ has a nearly sinusoidal waveform with the rms value of about 1.8 A. It lags to the line-to-line voltage by more than 30°. Fig. 12(c) shows the experimental waveforms of inductor current, dc-link current, and dc-link voltage during three switching cycles.

Fig. 13 shows the experiment results at the identical operating conditions with the simulation results shown in Fig. 10. As shown in Fig. 13, the dc-link voltage can be put up about 4.25 times from 50 V dc input voltage, and the ac output voltage and current, inductor and dc-link currents are decreased due to a lower shoot-through duty ratio. Fig. 14

describes the efficiency of the proposed MCA-ZSI with a variation of output power at the different shoot-through duty ratio. It can be noted that the proposed MCA-ZSI has more than 82% efficiency, and the efficiency at $D = 0.15$ is higher than that at $D = 0.2$.

In comparison to simulation results, the capacitor and dc-link voltages, and ac output voltage of the experimental results are slightly lower, owing to ESRs in the inductances and capacitances and the forward voltage drop of diodes and switching devices. It can be noted that the experimental results are nearly consistent with the simulation results and theoretical analysis.

## VI. Conclusions

This paper proposed a MCA-ZSI topology for improving the boost capability. Comparing with two different topologies based on switched ZSI, the proposed MCA-ZSI topology has higher boost factor, lower voltage stress across switching devices, and much lower voltage stress of four capacitors, while the total number of components used at the impedance network is identical with the other topologies. As validated by the experimental results, the dc-link voltage can be raised by about 6.8 times, and the ac output voltage with 185 Vrms can be generated from 50 V dc input voltage at a low shoot-through duty ratio of 0.214. The proposed MCA-ZSI has more than 82% efficiency. The proposed topology is suited to the renewal generation systems with a low voltage source.



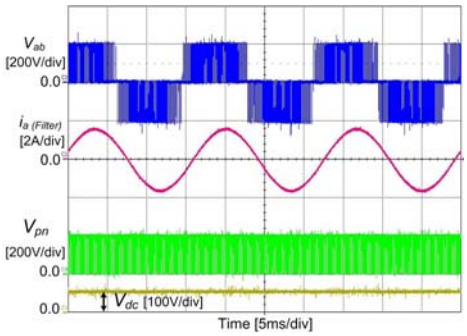


(a)

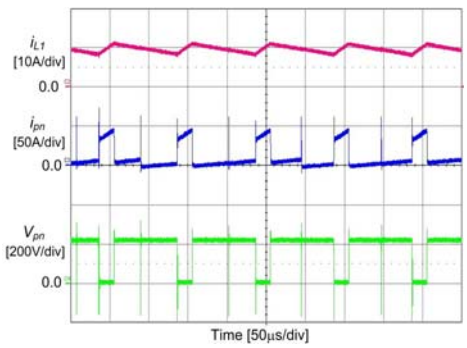


(b)

Fig. 13. Experimental results of MCA-ZSI at $M = 0.93$, $D = 0.195$: (a) ac output voltage and current, dc-link and dc input voltages, (b) inductor current, dc-link current and voltage.

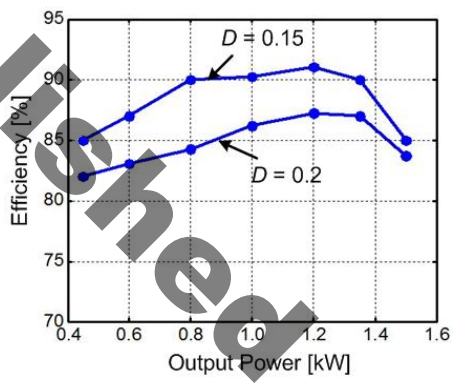


Fig. 14. Efficiency of MCA-ZSI with different shoot-through duty ratio.

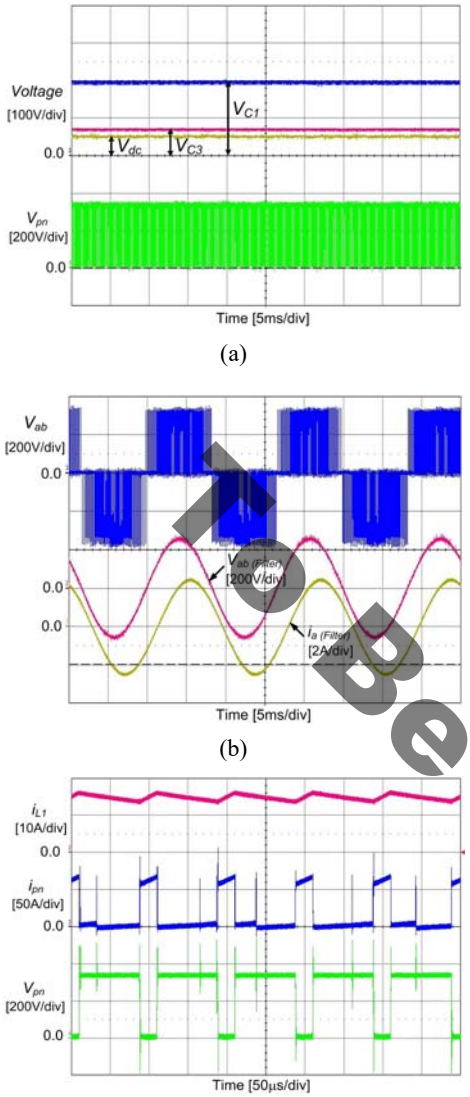


Fig. 12. Experimental results of MCA-ZSI at $M$ = 0.91, $D$ = 0.214: (a) two capacitor voltages, dc input and dc-link voltages, (b) ac output voltage, filtered ac output voltage, and phase current, (c) inductor current, dc-link current and voltage.



## ACKNOWLEDGMENT

This work was supported by the 2016 Research Fund of University of Ulsan.

## REFERENCES

[1] F. Z. Peng, "Z-source inverter," *IEEE Trans. Ind. Appl.*, vol. 39, no. 2, pp. 504–510, Mar. 2003.

[2] Z. Rymarski and K. Bernacki, "Influence of Z-source output impedance on dynamic properties of single-phase voltage source inverters for uninterrupted power supply," *IET Power Electron.*, vol. 7, no. 8, pp. 1978–1988, 2014.

[3] D. Vinnikov, A. Chub, E. Liivik, and I. Roasto, "High-performance quasi-Z-source series resonant DC–DC converter for photovoltaic module-level power electronics applications," *IEEE Trans. Power Electron.*, vol. 32, no. 5, pp. 3634-3650, May, 2017.

[4] Y. Liu, B. Ge, H. Abu-Rub, and F. Z. Peng, "An effective control method for three-phase quasi-Z-source cascaded multilevel inverter based grid-tie photovoltaic power system," *IEEE Trans. Ind. Electron.*, vol. 61, no. 12, pp. 6794–6802, Dec. 2014.

[5] C. L. Kala-Konga, M. N. Gitau, and R.C. Bansal, "Steady-state and small-signal models of a three-phase quasi-Z-source AC–DC converter for wind applications," *IET Renew. Power Gener.*, vol. 10, no. 7, pp. 1033–1040, 2016.

[6] H. Zhu, D. Yu, W. Zhu and Z. Zhou, "DC-link voltage regulation of bidirectional quasi-Z-source inverter for electric vehicle Applications," in *Proc. IEEE-VPPC*, 2016, pp.1-5.

[7] M. Zhu, K. Yu, and F. L. Luo, "Switched inductor Z-source inverter," *IEEE Trans. Power Electron.*, vol. 25, no. 8, pp. 2150-2158, Aug. 2010.

[8] H. Fathi and H. Madadi, "Enhanced-boost Z-source inverter with switched Z-impedance," *IEEE Trans. Ind. Electron.*, vol. 63, no. 2, pp. 691–703, Feb. 2016.

[9] M. K. Nguyen, Y. C. Lim, and G. B. Cho, "Switched-inductor quasi-Z-source inverter," *IEEE Trans. Power Electron.*, vol. 26, no. 11, pp. 3183-3191, Nov. 2011.

[10] K. Deng, J. Zheng, and J. Mei, "Novel switched-inductor quasi-Z-source inverter", *Journal of Power Electronics*, vol. 14, no. 1, pp. 11-21, Jan. 2014.

[11] M. K. Nguyen, Y. C. Lim, and J. H. Choi, "Two switched-inductor quasi-Z-source inverters," *IET Power Electron.*, vol. 5, no. 7, pp. 1017–1025, Aug. 2012.

[12] V. R. Vakacharla, M. Raghuram, and S. K. Singh, "Hybrid switched inductor impedance source converter-A decoupled approach," *IEEE Trans. Power Electron.*, vol. 31, no. 11, pp. 7509-7521, Nov. 2016.

[13] Y. P. Siwakoti, F. Z. Peng, F. Blaabjerg, P. C. Loh, and G. E. Town, "Impedance-source networks for electric power conversion part I: A topology review," *IEEE Trans. Power Electron.*, vol. 30, no. 2, pp. 699–716, Feb. 2015.

[14] Q. N. Trinh and H. H. Lee, "A new Z-source inverter topology with high voltage boost ability," *Journal of Elect. Eng. & Technology*, vol. 7, no. 5, pp. 714-723, 2012.

[15] D. Li, P. C. Loh, M. Zhu, F. Gao, and F. Blaabjerg, "Generalized multicell switched-inductor and switched-capacitor Z-source inverter," *IEEE Trans. Power Electron.*, vol. 28, no. 2, pp. 837-848, Feb. 2013.

[16] W. Qian, F. Z. Peng , and H. Cha, "Trans-Z-source inverters," *IEEE Trans. Power Electron.*, vol. 26, no. 12, pp. 3453–3463, Dec. 2011.

[17] S. D. Tavakoli, J. Khajesalehi, M. Hamzeh, and K. Sheshyekani, "Decentralised voltage balancing in bipolar dc microgrids equipped with trans-Z-source interlinking converter," *IET Renew. Power Gener.*, vol. 10, no. 5, pp. 703–712, 2016.

[18] S. Shubhra and S. Misha, "A coupled inductor based high boost inverter with sub-unity turns-ratio range," *IEEE*

*Trans. Power Electron.*, vol. 31, no. 11, pp. 7534-7543, Nov. 2016.

[19] M. K. Nguyen, Y. C. Lim, J. H. Choi, and Y. O. Choi, "Trans-switched boost inverters," *IET Power Electron.*, vol. 9, no. 5, pp. 1065–1073, 2016.

[20] Y. P. Siwakoti, F. Z. Peng, F. Blaabjerg, P. C. Loh, G. E. Town, and S. Yang, "Impedance-source networks for electric power conversion part II: Review of control and modulation techniques," *IEEE Trans. Power Electron.*, vol. 30, no. 4, pp. 1887–1906, Apr. 2015.

[21] M. Shen, J. Wang, A. Joseph, F. Z. Peng, L. M. Tolbert, and D. J. Adams, "Constant boost control of the Z-source inverter to minimize current ripple and voltage stress," *IEEE Trans. Ind. Appl.*, vol. 42, no. 3, pp. 770–778, May/Jun. 2006.

**Anh-Vu Ho** was born in Vietnam in 1981. He received the B.S. and M.S. degrees in electrical engineering from the HoChiMinh City University of Technical Education, Vietnam, in 2005 and 2009, respectively. He received the Ph. D. degree in electrical engineering at Ulsan University, Korea in 2015. He is a lecturer with the school of engineering, Eastern International University, Vietnam. His current research interests include power converter/inverter, power quality, and renewable energy system.

**Tae-Won Chun** was born in Korea in 1959. He received the B.S. degree in Electrical Engineering from Pusan National University in 1981, and received the M.S. and Ph.D. degrees in Electrical Engineering from Seoul National University in 1983 and 1987, respectively. Since 1986, he has been a member of the faculty of the Department of Electrical Engineering, Ulsan University, where he is currently a full Professor. He was with the Department of Electrical and Computer Engineering, University of Tennessee, USA as a visiting scholar. From 2005 to 2006, he also served as a visiting scholar with the Department of Electrical and Computer Engineering, Virginia Polytechnic Institute and State University, USA. His current research interests are the grid-connected inverter system and ac motor control.